

An integrated polyphenol-based hydrogel templating method for functional and structured oxidic nanomaterials

Marius Schöttle,^{+,†} Qingbo Xia,^{\$} Yen Theng Cheng,⁺ Nicholas D. Shepherd,^{\$} Chris D. Ling,^{,\$,±} and Markus Müller^{+,±,*}

⁺Key Centre for Polymers and Colloids, School of Chemistry, The University of Sydney, Sydney, NSW 2006, Australia.

^{\$}School of Chemistry, The University of Sydney, Sydney, NSW 2006, Australia. [±]The University of Sydney Nano Institute (Sydney Nano), Sydney, NSW 2006, Australia.

ABSTRACT: A straightforward fabrication method for tunable nanomaterials remains a key objective in the research areas of template chemistry, catalysis and energy storage materials. A growing focus in materials chemistry is the development of structuring methods that are simple, scalable, and at the same time include environmentally benign chemicals. We present a hydrogel-mediated templating method that yields customizable porous transition metal oxides. The protocol is extremely simple and includes predominantly naturally occurring compounds. For example, the incorporation of sacrificial polymer latex into a polyphenolic hydrogel network produces xerogel-composites with various filler content. Voids are generated simultaneously during pyrolysis of the dried gel, allowing for controlling the 3D arrangement of titania nanocrystals. As a proof-of-concept, we use the produced macroporous titania as a negative electrode (anode) material in lithium-ion batteries. We demonstrate that the gel-derived macroporous anatase significantly reduces the capacity loss compared to commercial or non-porous analogues. The modularity of this one-pot templating protocol is further demonstrated by the fabrication of titanate nanostructures and porous zirconia.

The need to improve various aspects of energy management and sustainable industrial procedures has become a driving force for collaborative research in materials science. One of the focal fields is the fabrication of functional architectures of oxidic compounds. This is highlighted by several high-impact reviews of their applications in gas-sensing,¹ heterogeneous catalysis^{2,3} and battery systems.⁴ Rapid implementation of the nanostructured oxides is naturally more likely if the synthesis procedure is simple, environmentally friendly and, ideally, variable. In this study, we focused primarily on titanium-based oxides and respective structuring methods thereof. The development of facile and less resource-demanding approaches to produce functional materials, such as TiO₂, covers a key focus in materials chemistry and related areas.

Classic sol-gel chemistry is widely used to prepare TiO₂, especially the anatase polymorph. Hydrolysis of alkoxide precursors can result in nanoparticles^{5,6} as well as nanoscale wires, tubes and sheets.⁷⁻¹⁰ More intricate structures such as mesoporous hollow spheres¹¹⁻¹³ or networks¹⁴⁻¹⁸ have also been realized. While there is extensive research dedicated to finding novel materials for battery components, we sought to highlight the continuous interest in the use and fabrication of titanium-containing nanomaterials. Anatase is a promising negative electrode (anode) material in lithium ion batteries (LIBs) with a theoretical capacity comparable to graphite.¹⁹ It is environmentally benign and inherently safe due to its high operating voltage.²⁰ However, its full potential can only be reached if length scales are reduced to the nanoscale while maintaining control over the superstructure.^{21,22} Aggregation and capacity loss during cycling can thereby be reduced while simultaneously enhancing the rate capability by improving the kinetics of charge and discharge.²³ Beside TiO₂, other promising oxides with a redox-active Ti(IV) species exist. An alternative anode material for LIBs is the lithium titanate Li₄Ti₅O₁₂. While it has a lower capacity than anatase, its cycling stability is exceptional.^{24,25} Compounds such as Na₂Ti₆O₁₃ and K₂Ti₈O₁₇ have also been applied in sodium and

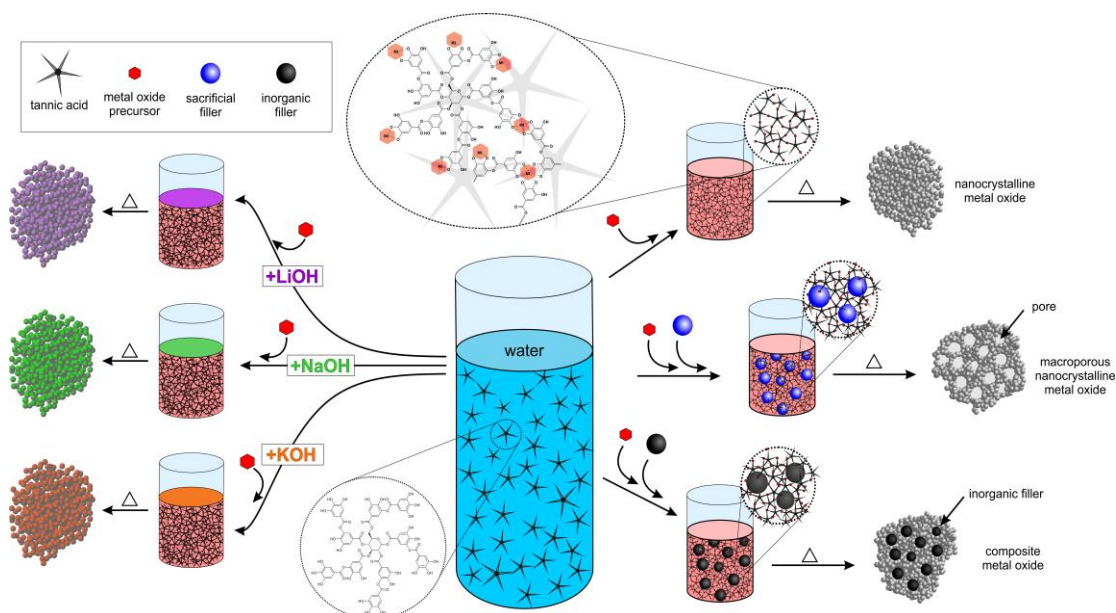
potassium ion batteries, respectively.²⁶⁻²⁸ Both show a lower capacity than TiO₂ in LIBs. However, the substitution of scarce lithium compounds makes this research essential for the long-term feasibility of energy storage using batteries.

Recently, Schnepf *et al.* proposed a broader definition of the term 'sol-gel chemistry'.²⁹ This includes ceramic materials produced by the Pechini method which exhibits a different gelling mechanism. An aqueous solution of a metal/citrate complex and ethylene glycol is heated to form a polyester network. The resulting hydrogel entraps metal oxide precursors in the homogeneous solution state. Calcination of the dried gels can produce various complex oxidic compounds.^{30,31} Variations of the Pechini method involve other carboxylic acids as complexing agents. Some showed the preparation of nanoscale titania and Li₄Ti₅O₁₂ and the potential as anode materials in LIBs.^{32,33} However, these usually include multiple steps to prepare a stable titanium precursor that does not prematurely hydrolyze. Carrying this idea forward, metal salts have been directly incorporated in polymeric hydrogels prior to calcination.^{34,35} The (bio-)polymer matrix significantly influences crystallization behavior and control the resulting particle size.³⁶

A similar type of chemistry is the use of precursors based on metal-organic frameworks (MOFs) prepared via crystallization of metal ions with multifunctional organic linkers. Several porous TiO₂ nanostructures were obtained by thermal decomposition of Ti-MOFs.^{37,38} Additionally, pyrolysis in an inert atmosphere was shown to result in oxide/carbon nanocomposites with an enhanced electric conductivity.³⁹

We introduce a new hydrogel-mediated method to titania and alkali metal titanate nanostructures (Scheme 1). Our study exploits

Scheme 1: Hydrogels formed by tannic acid and a metal precursor can be used in a facile templating route to produce nanocrystalline metal oxides (such as titania and zirconia). Mixing organic (sacrificial) or inorganic fillers into the hydrogel intermediate allows for producing porous or composite nanomaterials. The formation of titanium-based hydrogels in the presence of alkali hydroxides allows the production of a series of corresponding alkali metal titanates in the same one-pot procedure.



the possibility of forming hydrogels directly from titanium(IV) bis(ammonium lactate) dihydroxide (TALH) and polyphenols in one step.⁴⁰ The precursor TALH is a commercial, stable lactate-based titanium complex.^{41, 42} Titanium ions are directly chelated by tannic acid – a natural, molecular polyphenol – which in turn induces crosslinking and rapid but adjustable gelling.^{43, 44} Since gelling can be tuned, the addition of polystyrene particles as sacrificial fillers facilitates a simple, one-pot templating method toward macroporous nanocrystalline titania. We further assessed the application of the generated metal oxide structures as anode material in coin cell batteries, illustrating the importance of the interconnected structure achieved by our method by comparing them to commercial titania nanoparticles. We further demonstrate the modularity of this approach by feeding alkali metal hydroxides to the sol. Calcination thereby produces various titanates. Substituting TALH with a zirconia precursor enables the fabrication of structured ZrO_2 nanomaterials.

The underlying reaction in this work is a ligand exchange resulting in an interconnected hydrogel structure. Acetate ligands of the TALH (Ti^{4+}) complex are exchanged by the chelating polyphenolic moieties of tannic acid. This change in the chemical environment of the metal center can be directly observed as a color change from yellow to deep red caused by a ligand-to-metal charge transfer (LMCT). Gels made from tannic acid and various metal ions have been previously reported and their formation in several solvents has been thoroughly studied by Rahim *et al.*⁴⁰ Tannic acid is a star-shaped molecule with several anchor points. Its addition to the TALH solution therefore results in a loosely crosslinked network structure. The concomitant increase in viscosity, i.e. gelling, can be adjusted to proceed in a matter of minutes to facilitate further processing. An example for this is air-drying the hydrogel to produce a glassy red solid (xerogel) that can be converted into inorganic titania via calcination in air (Fig.S1). This method via a hydrogel intermediate lends itself for an extremely simple nanostructuring approach. Due to the controllable nature of the gelling reaction, different types of (nano-)particles can be added to the system. An illustration of the ease of generating composite materials is the addition of silica particles which results in a SiO_2/TiO_2 composite upon calcination (Fig. S2). Alternatively, polymer latex particles can be added to the hydrogel as a type of sacrificial filler that circumvents

the need for complex etching procedures when preparing porous materials. Simultaneous combustion of both the organic component of the xerogel as well as the sacrificial filler results in a foam-like, porous structure whereby the generated voids stem from the pyrolyzed fillers. This highlights the advantage of using a hydrogel intermediate, and differentiates it from other gel-based templating, as the metal precursor in this case acts as both the metal source and the crosslinking moiety. Further variability and modularity of this approach can be demonstrated by adding several alkali metal hydroxides prior to tannic acid addition. While these hydroxides do not interfere with the formation of the chelation complex, calcination of the corresponding gels resulted in a series of nanocrystalline titanates in contrast to pure titania without their addition.

In its simplest form, the presented process consists of air-drying the hydrogel to prepare a xerogel and a subsequent calcination step that results in pure, inorganic titania. When adding polystyrene latex particles as a sacrificial filler, the combustion taking place becomes more complex. To better understand the thermo-oxidative decomposition of all organic products, thermogravimetric analysis (TGA) of the various components was used (Fig. 1A).

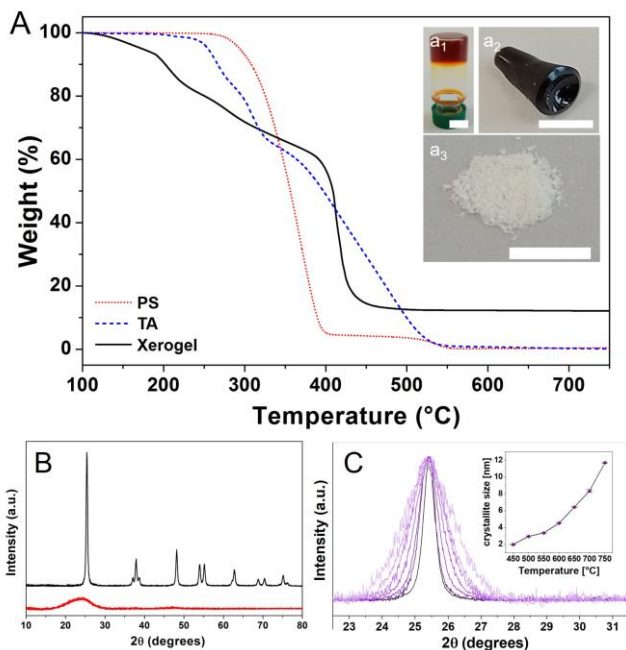


Figure 1: (A) Thermogravimetric analysis of the xerogel composite as well as separate measurements for the starting materials, including photographs of the hydrogel (inset, a₁), xerogel (inset, a₂) and inorganic titania residue after calcination (inset, a₃). (B) Powder X-ray diffraction (PXRD) patterns of the xerogel (red) and calcined TiO₂ product (black). (C) Broadening of the (101) reflection of anatase prepared at different temperatures, with an inset showing the evolution of the crystallite size as extracted from full Rietveld-refinements of the PXRD data using an isotropic particle size model.

Pure tannic acid decomposed completely in air. Weight loss began around 200 °C and completed at 550 °C. The Ti/tannic acid xerogel with incorporated polystyrene latex particles on the other hand showed weight loss beginning at slightly above 100 °C. This is attributed to residual water in the highly polar network. Weight loss in this case was completed at 450 °C showing a remainder of 13 wt.% corresponding to the inorganic residue. TGA analysis of pure polystyrene showed that the sacrificial filler decomposes in a similar temperature range as the organic linkers of the xerogel. We will nevertheless show a pronounced structure-directing effect thereof. Crystallographic insight into the formation of titania was obtained via powder X-ray diffraction (PXRD). The diffraction pattern of the xerogel exhibits only an amorphous halo between 20-30° 2θ (Fig. 1B). Unlike crystalline MOFs, this material has a flexible linker and most likely an inconsistent number of complexing catechol moieties per molecule of tannic acid which results in a disordered coordination polymer structure. The product of calcination in air at 750 °C was nanocrystalline anatase TiO₂. Temperature-dependent *ex situ* PXRD data were used to examine the evolution of the crystallite size (Fig. 1C). Full Rietveld refinements using an isotropic particle size model showed that between 500 – 750 °C the crystallite size increases from approximately 3 to 12 nm (Fig. 1C, inset). Further structural and electrochemical characterization will be limited to samples prepared at 750 °C. However, future optimization could include more extensive research into the calcination conditions.

The sacrificial filler used in this work is composed of monodisperse polystyrene latex particles prepared via an emulsifier-free emulsion polymerization (see Experimental Section). Scanning electron microscopy (SEM) images showed a uniform particle diameter of about 130 nm (Fig. 2A). The particles were prepared with acrylic acid as a comonomer which results in stabilization due to a

negative surface potential and compatibility with the tannic acid solution. No flocculation or aggregation was observed when the PS particles were mixed with tannic acid. We avoided other ionic moieties such as sulfonate groups as these could produce unwanted inorganic side phases upon calcination. The PS particles were incorporated into the xerogel by simple addition to the tannic acid solution and an otherwise unaltered gelling and air-drying process. A fractured surface of such a xerogel/polystyrene composite was examined by SEM (Fig. 2B). The composite surface exhibited a large number of holes where particles used to sit as well as the protruding particles themselves. While the particles were randomly distributed, no significant aggregation seemed to take place and particles were well dispersed in the xerogel matrix.

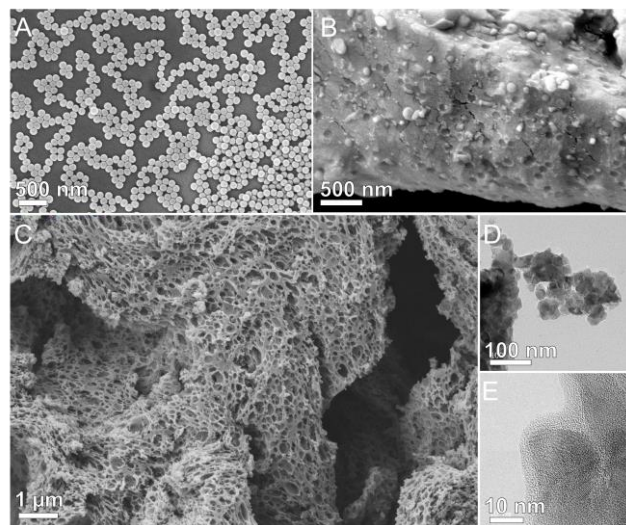


Figure 2: SEM images of (A) the polystyrene sacrificial filler particles, (B) the polystyrene particle/xerogel composite and (C) the titania nanofoam prepared via calcination. TEM images of the fragments of the structured titania at different magnifications (D/E).

Calcination of the composite was anticipated to produce a macroporous material due to simultaneous formation of nanocrystalline titania and the pore/void formation by the decomposing filler. A SEM image of the inorganic residue highlights an interconnected, foam-like, macroporous structure (Fig. 2C and Fig. S3/S4). The void diameter was predominantly between 100 – 200 nm, corroborating that these were formed as a consequence of the sacrificial filler. To further verify this, different amounts of filler were added to examine the effect on the porous structure (Fig. S5). Increasing filler content led to an increase in porosity, up to a point where significant coalescence could be observed. The 3D interconnected structure of nanocrystalline anatase is especially interesting due to the facile and green synthesis protocol. In a proof-of-concept study, we will show a viable application as an anode material in lithium ion batteries (LIBs), where the macroporous structure can significantly enhance the electrochemical cycling properties. An analysis of the structure on a smaller length scale was done beforehand using transmission electron microscopy (TEM). The smallest dimensions of the particles shown in Fig. 2D/E are consistent with the 12 nm obtained by Rietveld-refinement (note that the smallest dimension typically dominates the broadening in XRD). Beside the crystalline core, a seemingly amorphous phase was observed enclosing the former. An amorphous titania matrix, filling voids between anatase particles, explained the relatively small surface area of 14 m²·g⁻¹ and the absence of micro- and mesopores as seen in physisorption experiments (Fig. S6). The accessible surface area must therefore be predominantly attributed to the macropores. Incomplete crystallization, entailing an amorphous side-phase, was most likely caused by

a rather short calcination time of only 60 minutes. Summing up the synthesis protocol, the structural characterization indicated that our hydrogel mediated approach produces a composite of nanocrystalline anatase in an amorphous TiO_2 matrix with a macroporous, sponge-like superstructure.

Coin cells using the macroporous titania (MPT) as the anode were prepared to examine its electrochemical properties. Analogously, comparison cells were fabricated using commercial anatase nanoparticles (P25 nanopowder, 21 nm primary particle size). Charge/discharge curves and cycling stability measurements of both were obtained (Fig. 3A/B). The initial discharge capacity of the commercial anatase was nearly twice that of the MPT (Fig. S7) which is attributed to more side-reactions with the electrolyte due to the greater surface area. The commercial anatase showed a pronounced irreversible capacity loss, with the discharge capacity dropping from $300 \text{ mAh}\cdot\text{g}^{-1}$ to $170 \text{ mAh}\cdot\text{g}^{-1}$ after 15 cycles and to $150 \text{ mAh}\cdot\text{g}^{-1}$ ($\sim 50\%$ capacity loss) after 100 cycles. The MPT in contrast exhibited a much greater cycling stability. Starting at a slightly lower discharge capacity of $250 \text{ mAh}\cdot\text{g}^{-1}$, the templated MPT showed a significantly reduced capacity loss ($<10\%$) to $225 \text{ mAh}\cdot\text{g}^{-1}$ after 100 cycles. The coulombic efficiency was close to 100 % throughout the entire process. With the interconnected 3D macroporous structure effectively being the only difference between the materials, we corroborate that the MPT prepared via the hydrogel approach enhances battery cycling stability. While the commercial nanoparticles formed aggregates during the first cycles, the MPT can accommodate structural and volumetric changes and thereby prevents the consequential capacity loss. SEM images before and after cycling show that the foam-like superstructure remains intact during the 100 cycling steps (Fig. S8). Rate capability measurements (Fig. 3C) between 0.1 – 4 C show a stepwise decrease to $80 \text{ mAh}\cdot\text{g}^{-1}$. When reducing the current back to 0.1 C, the capacity returns to the initial high value close to $250 \text{ mAh}\cdot\text{g}^{-1}$. The necessity of a macroporous structure was further underlined when electrochemical cycling data of titania prepared with the hydrogel method but without a sacrificial filler was examined (Fig. S9). In this case the discharge capacity starts at around $150 \text{ mAh}\cdot\text{g}^{-1}$ and remains constant. This corresponds well with the behavior expected for bulk anatase.

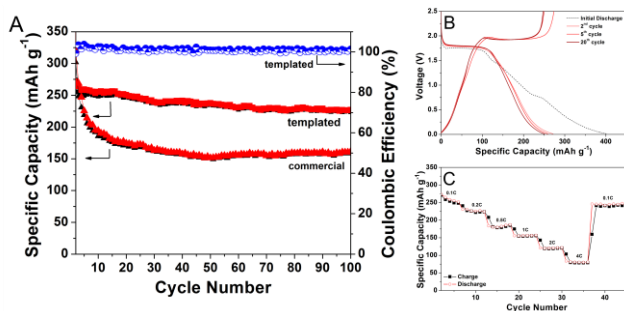


Figure 3: (A,B) Electrochemical cycling of the macroporous titania; (B) shows the initial discharge as well as the 2nd, 5th, and 20th cycle. (C) Rate capability measurements at 0.1, 0.2, 0.5, 1, 2 and 4C.

These measurements demonstrate how our one-pot hydrogel-mediated structuring method endows titania with beneficial properties in lithium ion battery anodes. To showcase the variability of this method, more complex ionic compounds were prepared. By simple addition of alkali metal hydroxides to the tannic acid solution prior to gelling, it is possible to prepare several types of titanates in a straightforward manner. We also characterized these titanates with PXRD and SEM (Fig. 4). Hydroxide addition had no adverse effects with respect to the gelling reaction. The formation of a chelate complex with a distinct LMCT was examined with UV-vis spectroscopy (Fig. S10) and no differences between the systems

could be detected. Addition of LiOH and subsequent calcination led to the formation of a lithium titanate, $\text{Li}_4\text{Ti}_5\text{O}_{12}$, which has also been shown to be applicable as an anode material in LIBs.⁴⁵ SEM images of the material showed aggregates of irregular shaped nanoparticles. No anisotropy or preferred growth could be observed (Fig. 4A,D).

In contrast, sodium titanate prepared by addition of NaOH instead showed a directed crystal growth. Aggregates of rod-shaped $\text{Na}_2\text{Ti}_6\text{O}_{13}$ nanocrystallites were formed upon calcination (Fig. 4B,E). We attribute the anisotropic growth to the highly anisotropic unit cell of the sodium titanate. $\text{Na}_2\text{Ti}_6\text{O}_{13}$ shows 1D transport of sodium ions and can therefore be applied as an anode material in sodium ion batteries (SIBs). We prepared coin-cells with our material and obtained a stable cycling performance with a reversible capacity of $90 \text{ mAh}\cdot\text{g}^{-1}$ (Fig. S11), which falls in the range of previously published values.²⁷

A third structure, the potassium titanate $\text{K}_2\text{Ti}_8\text{O}_{17}$, was prepared by simply adding KOH. Calcination produced aggregated crystallites with a similar morphology compared to the sodium titanate (Fig. 4C,F). This further corroborates the tunnel-like structure being the reason for this anisotropic growth, as the two compounds have a similar crystal structure. $\text{K}_2\text{Ti}_8\text{O}_{17}$ has also been reported as a suitable anode material; albeit in the less examined class of potassium ion batteries.²⁸ Looking forward, a focused study on using our novel method for preparing titanates with an adjustable nano- and mesostructure could provide further insight into their use in batteries and investigate potential structure-based performance enhancements. Regardless, we were able to synthesize valuable titanates using the same one-pot, hydrogel-mediated method as described above. Similarly, facile optimization of these materials is warranted through our sacrificial filler approach.

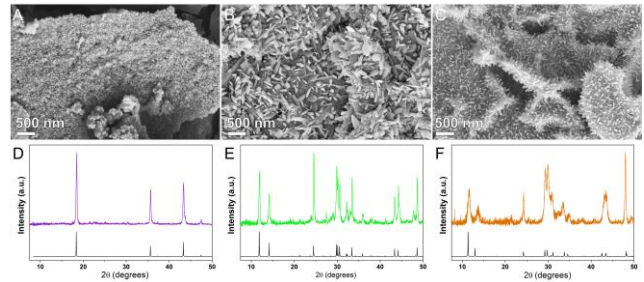


Figure 4: SEM images and PXRD patterns of the lithium- (A/D), sodium- (B/E) and potassium-titanates (C/F).

Finally, we sought to investigate whether other cations besides Ti^{4+} can be applied in our synthesis protocol. Both hydrogel preparation and the sacrificial templating route were tested using a zirconia precursor. We prepared hydrogels with ZrOCl_2 as the Zr^{4+} precursor and continued to use the polystyrene latex particles as a sacrificial filler. Zr^{4+} can form an analogous hydrogel with tannic acid. Air-drying and subsequent calcination at 750°C for 60 min produced a white powder, for which the PXRD pattern revealed a mixture of tetragonal and cubic ZrO_2 (Fig. 5) – a commonly reported composition for zirconia prepared via combustion methods.^{46,47} More importantly, SEM images confirmed the presence of macroporous structure, similar to MPT. This underlines the structure-directing effect of the sacrificial filler and demonstrates that our approach is applicable to different systems to open a range of future possibilities in the fabrication of structured zirconates, mixtures of titania and zirconia or possibly other transition metal oxides.

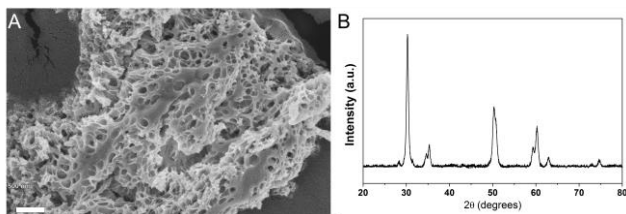


Figure 5: (A) SEM image and (B) PXRD pattern of zirconia nanofoam (mixed polymorph of cubic and tetragonal crystal structure) after calcination.

In conclusion, we presented a polyphenol-based hydrogel templating method as a versatile new approach to yield various metal oxide nanomaterials with tailored porosity and composition. The fabrication proceeds via a simple gelation step in water using commercially available, non-toxic components followed by drying and a short heat treatment. The gel network was established directly via metal-ligand exchange between a metal precursor and tannic acid. The introduction of additional molecules (alkali bases) or particulates (silica or polystyrene) did not hamper gel formation and could in fact be used to alter the final product. The introduction of porosity was shown to be beneficial for cycling stability in LIB, while the fabrication of templated titanates or zirconia may be further explored in other energy storage applications. This proof-of-concept study demonstrated a modular structuring method that can be easily adopted to produce various oxidic nanostructures from mainly ecologically benign starting materials in an economically favorable process. We anticipate that this templating approach can be further developed into a multipurpose platform technology for metal oxide synthesis and used in parallel to current standard procedures, such as hydrothermal synthesis routes.

EXPERIMENTAL SECTION

Materials. The following reagents and chemicals were sourced from Sigma-Aldrich Australia: styrene (>99%), acrylic acid (99%), tannic acid (>87%), zirconyl chloride octahydrate (>98%), titanium(IV) bis(ammonium lactato)dihydroxide (TALH) solution (50 wt.% in water), nanosized anatase particles (P25, 99.7%), polyvinylidene fluoride (PVDF, >99%) and 1M lithium hexafluorophosphate electrolyte solution in ethylene carbonate/diethyl carbonate (1:1). Carbon black (>99%) and 1-methyl 2-pyrrolidinone (NMP) (>99%) was received from Alfa Aesar. LiOH, NaOH and KOH pellets as well as dimethyl sulfoxide (DMSO) (>95%) were obtained from Ajax. Potassium persulfate (>99%) was sourced from Merck. Water used in this work was of MilliQ quality. Coin cell sets were purchased from MTI and included stainless steel 2032 top and bottom caps, wave springs, spacers and 19 mm Celgard polypropylene separator films.

Characterization. Thermogravimetric analysis (TGA) was performed on a TA Instruments Discovery thermogravimetric analyzer. Samples were heated under a flow of air from room temperature to 550 °C (or otherwise desired temperature) at a ramp rate of 5 °C/min. The samples were held at 110 °C for 15 min to remove residual solvent. Powder X-ray Diffraction (PXRD) data were collected on a PANalytical X-pert Pro powder diffractometer, with Cu K α X-ray radiation and a PIXcel1D detector in continuous scanning mode at a speed of 1.26°/min over the 2 θ angle range 5-80°. Transmission electron microscopy (TEM) was performed on a JEOL 2200FS instrument in bright field mode with a spot size of 3, operating at an accelerating voltage of 200 kV using a 2k x 2k Ultrascan 1000XP CCD camera (Gatan). Images were processed with the Digital Micrograph software. The mesostructured titania powders were well-dispersed in ethanol by ultrasonic and then loaded on the ultra-thin carbon film which is supported by the copper grid. Scanning electron microscopy (SEM) was conducted on a Zeiss Sigma HD FEG SEM. Images were collected at a working distance

of 3.7-5.1 mm at an accelerating voltage of 5 kV. All samples were sputtered with gold (15 nm) prior to imaging unless stated otherwise. N $_2$ -isotherms were recorded at 77 K on a 3Flex Surface Characterisation Analyser (Micromeritics Instruments Inc.). Prior to this, samples were outgassed under dynamic vacuum ($\sim 10^{-6}$ bar) at 100°C for 20 hours. The S $_{BET}$ values were calculated with BET theory⁴⁸ using 3Flex software (version 4.01, Micromeritics Instrument Corporation).

Emulsifier Free Emulsion Polymerization. A simple type of polystyrene (PS) nanoparticle synthesis was chosen for this work.⁴⁹ In an emulsifier free emulsion polymerization, a three-neck flask equipped with a reflux condenser was loaded with 80 mL MilliQ water, 10 mL styrene and 0.3 mL acrylic acid. After heating to 75 °C with an oil bath, the system was purged with nitrogen while stirring at 850 rpm for 60 minutes. The polymerization was initiated by adding 5 mg potassium persulfate in 3 mL MilliQ water under nitrogen flow. The reaction was stirred under constant nitrogen flow over night after which termination ensued by exposure to ambient oxygen and cooled to room temperature. PS nanoparticle dispersions were diluted with MilliQ water prior to further use in templating procedures.

Gel-templated Titania Preparation. In a typical hydrogel preparation, a solution of 500 mg (0.295 mmol) tannic acid in 12.5 mL MilliQ water was prepared. The TALH solution (as received) was diluted with DMSO before further use (TALH/DMSO = 4:1, v/v). To the tannic acid solution, 875 μ L of TALH/DMSO solution was added, immediately vortexed for 10 seconds and left to stand still for 4 hours. In this time the gelling reaction could proceed after which the resulting hydrogels were frozen with liquid nitrogen and freeze dried (or dried in air) for 48 hours. The dried, red xerogel was transferred into a furnace in alumina crucibles and heated at 3.7 °C/min to 750 °C in air. The sample was kept at this temperature for 60 minutes and subsequently cooled to room temperature. The respective titania was obtained as a white powder.

Hydrogel Preparation and Conversion to Titanates. In a typical hydrogel preparation, a solution of 500 mg (0.295mmol) tannic acid in 12.5 mL MilliQ water was mixed with 1.25 mL of an aqueous 1M solution of either LiOH, NaOH or KOH. The as obtained TALH solution was diluted with DMSO before further use (TALH/DMSO = 4:1, v/v). To the tannic acid solution with LiOH, 625 μ L TALH solution was added. Twice this amount (1250 μ L TALH solution) was added to the tannic acid solutions with NaOH and KOH. In all cases the solution was immediately vortexed for 10 seconds and left to stand still for 4 hours. In this time the gelling reaction could proceed after which the resulting hydrogels were frozen with liquid nitrogen and freeze dried for 48 hours. After drying the orange/red samples were transferred into a furnace in alumina crucibles. At 3.7 °C/min they were heated to 750 °C in air and kept at this temperature for 60 minutes and subsequently cooled to room temperature. The respective titanates were all obtained as white powders.

Templating of Titania and Zirconia via Latex/Hydrogel Nanocomposites. Macroporous titania structures were prepared in a similar manner to the alkali metal titanates. 500 mg tannic acid were dissolved in 12.5 mL of an aqueous PS latex particle dispersion (0.5 wt.%, 625 mg PS). Addition of 875 μ L of the diluted TALH solution was followed by immediate vortexing for 10 seconds. The system was left to stand still for 4 hours and subsequently air dried at 50 °C for approximately 4 days. The following calcination proceeded analogously to the titanate synthesis. Macroporous zirconia was prepared analogously with 20 mg tannic acid dissolved in 350 μ L of the same PS dispersion. This was added to 19 mg ZrOCl $_2$ x 8H $_2$ O dissolved in 150 μ L MilliQ water and resulted in a light-yellow hydrogel. The drying and calcination process remained the same.

Coin Cell Fabrication and Testing. The slurry for electrode preparation was prepared by mixing the nanostructured anatase (140 mg), carbon black (30 mg) and PVDF (30 mg) with 2 mL NMP and stirring overnight. This was coated on a clean copper foil via doctor-blading with a blade height of 20 μm . After drying overnight at 80 $^{\circ}\text{C}$, electrodes were prepared by cutting discs out of the coated copper foil. Assembly of coin cells occurred in an argon filled glove box. The respective layers were arranged (bottom to top) in the following order: bottom case, anode (copper side facing down), separator, electrolyte solution, lithium metal, spacer, wave spring and top case. The finished coin cells were cycled and analyzed using a Neware battery testing system in a voltage window of 0.01 V to 2.5 V and 1.0 V to 2.5 V, respectively. The fabrication procedures of sodium-ion half-cells are same with that of Li-cells but sodium metal and 1M NaClO₄ solution (which has same solvents with that of the LiFP₆ electrolyte) are used as counter electrodes and the electrolyte, respectively.

ASSOCIATED CONTENT

Supporting Information

The Supporting Information is available free of charge on the ACS Publications website. Supporting Information includes further microscopy analyses, physisorption and spectroscopic measurements, and additional electrochemical performance studies.

AUTHOR INFORMATION

Corresponding Author

E-mail: markus.muellner@sydney.edu.au

Present Addresses

† Physical Chemistry I, University of Bayreuth, Universitätsstr. 30, 95447 Bayreuth, Germany.

Author Contributions

All authors have given approval to the final version of the manuscript.

ACKNOWLEDGMENT

This research was facilitated by access to Sydney Analytical, a core research facility at the University of Sydney. M.S. acknowledges the Elite Network Bavaria. Y.T.C. is a grateful recipient of a University of Sydney International Scholarship (USyDIS). M.M. and C.D.L. acknowledge the Australian Research Council for a Discovery Early Career Researcher Award (DE180100007) and Discovery Project (DP170100269), respectively.

REFERENCES

- Li, Z.; Li, H.; Wu, Z.; Wang, M.; Luo, J.; Torun, H.; Hu, P.; Yang, C.; Grundmann, M.; Liu, X.; Fu, Y., Advances in designs and mechanisms of semiconducting metal oxide nanostructures for high-precision gas sensors operated at room temperature. *Mater. Horiz.* **2019**, *6* (3), 470-506.
- Xia, Z.; An, L.; Chen, P.; Xia, D., Non-Pt Nanostructured Catalysts for Oxygen Reduction Reaction: Synthesis, Catalytic Activity and its Key Factors. *Adv. Energy Mater.* **2016**, *6* (17), 1600458.
- Zhang, S.; Zhao, Y.; Shi, R.; Waterhouse, G. I. N.; Zhang, T., Photocatalytic ammonia synthesis: Recent progress and future. *Energy Chem* **2019**, *1* (2), 100013.
- Zheng, M.; Tang, H.; Li, L.; Hu, Q.; Zhang, L.; Xue, H.; Pang, H., Hierarchically Nanostructured Transition Metal Oxides for Lithium-Ion Batteries. *Adv. Sci.* **2018**, *5* (3), 1700592.
- Selvaraj, P.; Roy, A.; Ullah, H.; Sujatha Devi, P.; Tahir, A. A.; Mallick, T. K.; Sundaram, S., Soft-template synthesis of high surface area mesoporous titanium dioxide for dye-sensitized solar cells. *Int. J. Energy Res.* **2019**, *43* (1), 523-534.
- Sushko, M. L.; Rosso, K. M.; Liu, J., Size Effects on Li⁺/Electron Conductivity in TiO₂ Nanoparticles. *J. Phys. Chem. Lett.* **2010**, *1* (13), 1967-1972.
- Acar, H.; Garifullin, R.; Guler, M. O., Self-Assembled Template-Directed Synthesis of One-Dimensional Silica and Titania Nanostructures. *Langmuir* **2011**, *27* (3), 1079-1084.
- Müllner, M.; Lunkenbein, T.; Miyajima, N.; Breu, J.; Müller, A. H. E., A Facile Polymer Templating Route Toward High-Aspect-Ratio Crystalline Titania Nanostructures. *Small* **2012**, *8* (17), 2636-2640.
- Kluson, P.; Luskova, H.; Solcova, O.; Matejova, L.; Cajthaml, T., Lamellar micelles-mediated synthesis of nanoscale thick sheets of titania. *Mater. Lett.* **2007**, *61* (14), 2931-2934.
- Chae, W.-S.; Lee, S.-W.; Kim, Y.-R., Templating Route to Mesoporous Nanocrystalline Titania Nanofibers. *Chem. Mater.* **2005**, *17* (12), 3072-3074.
- Sasidharan, M.; Nakashima, K., Core-Shell-Corona Polymeric Micelles as a Versatile Template for Synthesis of Inorganic Hollow Nanospheres. *Acc. Chem. Res.* **2014**, *47* (1), 157-167.
- Wang, H.-E.; Jin, J.; Cai, Y.; Xu, J.-M.; Chen, D.-S.; Zheng, X.-F.; Deng, Z.; Li, Y.; Bello, I.; Su, B.-L., Facile and fast synthesis of porous TiO₂ spheres for use in lithium ion batteries. *J. Coll. Interface Sci.* **2014**, *417*, 144-151.
- Zhang, G.; Wu, H. B.; Song, T.; Paik, U.; Lou, X. W., TiO₂ Hollow Spheres Composed of Highly Crystalline Nanocrystals Exhibit Superior Lithium Storage Properties. *Angew. Chem. Int. Ed.* **2014**, *53* (46), 12590-12593.
- Zhang, D.; Qi, L., Synthesis of mesoporous titania networks consisting of anatase nanowires by templating of bacterial cellulose membranes. *Chem. Commun.* **2005**, (21), 2735-2737.
- Brendel, J. C.; Lu, Y.; Thelakkat, M., Polymer templated nanocrystalline titania network for solid state dye sensitized solar cells. *J. Mater. Chem.* **2010**, *20* (34), 7255-7265.
- Lui, G.; Li, G.; Wang, X.; Jiang, G.; Lin, E.; Fowler, M.; Yu, A.; Chen, Z., Flexible, three-dimensional ordered macroporous TiO₂ electrode with enhanced electrode-electrolyte interaction in high-power Li-ion batteries. *Nano Energy* **2016**, *24*, 72-77.
- Kimling, M. C.; Caruso, R. A., Sol-gel synthesis of hierarchically porous TiO₂ beads using calcium alginate beads as sacrificial templates. *J. Mater. Chem.* **2012**, *22* (9), 4073-4082.
- Chee Kimling, M.; Scales, N.; Hanley, T. L.; Caruso, R. A., Uranyl-Sorption Properties of Amorphous and Crystalline TiO₂/ZrO₂ Millimeter-Sized Hierarchically Porous Beads. *Environm. Sci. Technol.* **2012**, *46* (14), 7913-7920.
- Chen, Z.; Belharouak, I.; Sun, Y.-K.; Amine, K., Titanium-Based Anode Materials for Safe Lithium-Ion Batteries. *Adv. Funct. Mater.* **2013**, *23* (8), 959-969.
- Wang, D.; Choi, D.; Li, J.; Yang, Z.; Nie, Z.; Kou, R.; Hu, D.; Wang, C.; Saraf, L. V.; Zhang, J.; Aksay, I. A.; Liu, J., Self-Assembled TiO₂-Graphene Hybrid Nanostructures for Enhanced Li-Ion Insertion. *ACS Nano* **2009**, *3* (4), 907-914.
- Wagemaker, M.; Borghols, W. J. H.; Mulder, F. M., Large Impact of Particle Size on Insertion Reactions. A Case for Anatase Li_x-TiO₂. *J. Am. Chem. Soc.* **2007**, *129* (14), 4323-4327.
- Wagemaker, M.; Kearley, G. J.; van Well, A. A.; Mutka, H.; Mulder, F. M., Multiple Li Positions inside Oxygen Octahedra in Lithiated TiO₂ Anatase. *J. Am. Chem. Soc.* **2003**, *125* (3), 840-848.
- Wang, K.; Wei, M.; Morris, M. A.; Zhou, H.; Holmes, J. D., Mesoporous Titania Nanotubes: Their Preparation and Application as Electrode Materials for Rechargeable Lithium Batteries. *Adv. Mater.* **2007**, *19* (19), 3016-3020.
- Wang, C.; Wang, S.; Tang, L.; He, Y.-B.; Gan, L.; Li, J.; Du, H.; Li, B.; Lin, Z.; Kang, F., A robust strategy for crafting monodisperse Li₄Ti₅O₁₂ nanospheres as superior rate anode for lithium ion batteries. *Nano Energy* **2016**, *21*, 133-144.
- Liu, J.; Song, K.; van Aken, P. A.; Maier, J.; Yu, Y., Self-Supported Li₄Ti₅O₁₂-C Nanotube Arrays as High-Rate and Long-Life Anode Materials for Flexible Li-Ion Batteries. *Nano Lett.* **2014**, *14* (5), 2597-2603.
- Cao, K.; Jiao, L.; Pang, W. K.; Liu, H.; Zhou, T.; Guo, Z.; Wang, Y.; Yuan, H., Na₂Ti₆O₁₃ Nanorods with Dominant Large Interlayer

- Spacing Exposed Facet for High-Performance Na-Ion Batteries. *Small* **2016**, *12* (22), 2991-2997.
27. Rudola, A.; Saravanan, K.; Devaraj, S.; Gong, H.; Balaya, P., Na₂Ti₅O₁₃: a potential anode for grid-storage sodium-ion batteries. *Chem. Commun.* **2013**, *49* (67), 7451-7453.
 28. Han, J.; Xu, M.; Niu, Y.; Li, G.-N.; Wang, M.; Zhang, Y.; Jia, M.; Li, C. m., Exploration of K₂Ti₈O₁₇ as an anode material for potassium-ion batteries. *Chem. Commun.* **2016**, *52* (75), 11274-11276.
 29. Danks, A. E.; Hall, S. R.; Schnepf, Z., The evolution of 'sol-gel' chemistry as a technique for materials synthesis. *Mater. Horiz.* **2016**, *3* (2), 91-112.
 30. Abreu, A.; Zanetti, S. M.; Oliveira, M. A. S.; Thim, G. P., Effect of urea on lead zirconate titanate—Pb(Zr_{0.52}Ti_{0.48})O₃—nanopowders synthesized by the Pechini method. *J. Eur. Cer. Soc.* **2005**, *25* (5), 743-748.
 31. Pechini, M. P. Method of Preparing Lead and Alkaline Earth Titanates and Niobates and Coating Method Using the Same to Form a Capacitor. 1967.
 32. Zhou, Y.; Lee, J.; Lee, C. W.; Wu, M.; Yoon, S., Crystallinity-Controlled Titanium Oxide–Carbon Nanocomposites with Enhanced Lithium Storage Performance. *ChemSusChem* **2012**, *5* (12), 2376-2382.
 33. Zhang, C.; Zhang, Y.; Wang, J.; Wang, D.; He, D.; Xia, Y., Li₄Ti₅O₁₂ prepared by a modified citric acid sol-gel method for lithium-ion battery. *J. Power Sources* **2013**, *236*, 118-125.
 34. Schnepf, Z.; Hollamby, M. J.; Tanaka, M.; Matsushita, Y.; Xu, Y.; Sakka, Y., A family of oxide-carbide-carbon and oxide-nitride-carbon nanocomposites. *Chem. Commun.* **2014**, *50* (40), 5364-5366.
 35. Schnepf, Z.; Thomas, M.; Glatzel, S.; Schlichte, K.; Palkovits, R.; Giordano, C., One pot route to sponge-like Fe₃N nanostructures. *J. Mater. Chem.* **2011**, *21* (44), 17760-17764.
 36. Schnepf, Z.; Hall, S. R.; Hollamby, M. J.; Mann, S., A flexible one-pot route to metal/metal oxide nanocomposites. *Green Chem.* **2011**, *13* (2), 272-275.
 37. Wang, Z.; Li, X.; Xu, H.; Yang, Y.; Cui, Y.; Pan, H.; Wang, Z.; Chen, B.; Qian, G., Porous anatase TiO₂ constructed from a metal-organic framework for advanced lithium-ion battery anodes. *J. Mater. Chem. A* **2014**, *2* (31), 12571-12575.
 38. Xu, X.; Cao, R.; Jeong, S.; Cho, J., Spindle-like Mesoporous α-Fe₂O₃ Anode Material Prepared from MOF Template for High-Rate Lithium Batteries. *Nano Lett.* **2012**, *12* (9), 4988-4991.
 39. Niu, P.; Wu, T.; Wen, L.; Tan, J.; Yang, Y.; Zheng, S.; Liang, Y.; Li, F.; Irvine, J. T. S.; Liu, G.; Ma, X.; Cheng, H.-M., Substitutional Carbon-Modified Anatase TiO₂ Decahedral Plates Directly Derived from Titanium Oxalate Crystals via Topotactic Transition. *Adv. Mater.* **2018**, *30* (20), 1705999.
 40. Rahim, M. A.; Björnalm, M.; Suma, T.; Faria, M.; Ju, Y.; Kempe, K.; Müllner, M.; Ejima, H.; Stickland, A. D.; Caruso, F., Metal-Phenolic Supramolecular Gelation. *Angew. Chem Int. Ed.* **2016**, *55* (44), 13803-13807.
 41. McRae, O. F.; Xia, Q.; Tjaberings, S.; Gröschel, A. H.; Ling, C. D.; Müllner, M., Block copolymer-directed synthesis of porous anatase for lithium-ion battery electrodes. *J. Polym. Sci. Part A: Polym. Chem.* **2019**, *57* (18), 1890-1896.
 42. Müllner, M.; Lunkenbein, T.; Schieder, M.; Gröschel, A. H.; Miyajima, N.; Förtsch, M.; Breu, J.; Caruso, F.; Müller, A. H. E., Template-Directed Mild Synthesis of Anatase Hybrid Nanotubes within Cylindrical Core-Shell-Corona Polymer Brushes. *Macromolecules* **2012**, *45* (17), 6981-6988.
 43. Rahim, M. A.; Ejima, H.; Cho, K. L.; Kempe, K.; Müllner, M.; Best, J. P.; Caruso, F., Coordination-Driven Multistep Assembly of Metal-Polyphenol Films and Capsules. *Chem. Mater.* **2014**, *26* (4), 1645-1653.
 44. Rahim, M. A.; Kristufek, S. L.; Pan, S.; Richardson, J. J.; Caruso, F., Phenolic Building Blocks for the Assembly of Functional Materials. *Angew. Chem. Int. Ed.* **2019**, *58* (7), 1904-1927.
 45. Zhao, B.; Ran, R.; Liu, M.; Shao, Z., A comprehensive review of Li₄Ti₅O₁₂-based electrodes for lithium-ion batteries: The latest advancements and future perspectives. *Mater. Sci. Eng. Reports* **2015**, *98*, 1-71.
 46. Keitab, A. S.; Saion, E.; Zakaria, A.; Soltani, N., Structural and Optical Properties of Zirconia Nanoparticles by Thermal Treatment Synthesis. *J. Nanomater.* **2016**, 1913609
 47. Wang, Q.; Li, C.; Guo, M.; Hu, C.; Xie, Y., Controllable synthesis of zirconia nano-powders using vapor-phase hydrolysis and theoretical analysis. *J. Mater. Chem. A* **2014**, *2* (5), 1346-1352.
 48. Brunauer, S.; Emmett, P.H.; Teller, E., Adsorption of gases in multimolecular layers. *J. Am. Chem. Soc.* **1938**, *60*, 309-319.
 49. Nutz, F. A.; Ruckdeschel, P.; Retsch, M., Polystyrene colloidal crystals: Interface controlled thermal conductivity in an open-porous mesoparticle superstructure. *J. Colloid Inter. Sci.* **2015**, *457*, 96-101.

